Microchim Acta Volume 187, December 2020, Article number 657
DOI:10.1007/s00604-020-04624-w

Subsequent monitoring of ferric ion and ascorbic acid using graphdiyne quantum dots-based optical sensors

Qiang Bai[a,c], Chaoyang Zhang[b], Long Li[b], Zhiling Zhu[a], Lina Wang[b,*], Fuyi Jiang[c], Manhong Liu[a], Zhaobo Wang[a], William W. Yu [a,d], Fanglin Du[a,*], Zhugen Yang[e,*], Ning Sui[a,*]

[a] College of Materials Science and Engineering, Qingdao University of Science and Technology, Qingdao 266042, China

[b] College of Environment and Safety Engineering, Qingdao University of Science and Technology, Qingdao, 266042, China.

[c] School of Environment and Material Engineering, Yantai University, Yantai, 264005, Shandong, China

[d] Department of Chemistry and Physics, Louisiana State University Shreveport, LA 71115, USA

[e] Cranfield Water Science Institute, Cranfield University, Milton Keynes, MK43 0AL, United Kingdom

* Corresponding authors: suining@qust.edu.cn (N. Sui), lnwang2006@163.com (L.N. Wang), dufanglin@qust.edu.cn (F.L. Du), zhugen.yang@cranfield.ac.uk (Z.G. Yang)

Abstract

Graphdiyne (GDY) as an emerging carbon nanomaterial has attracted increasing attention because of its uniformly distributed pores, highly π-conjugated, and tunable electronic properties. These excellent characteristics have been widely explored in the fields of energy storage, catalysts, there is yet report on the sensors development based on its outstanding optical property. In this paper, we report on a new sensing mechanism built upon the synergistic effect between inner filter effect and photoinduced electron transfer. We constructed a novel nanosensor based upon the newly-synthesized nanomaterial and demonstrated a sensitive and selective detection for both ion (Fe^{3+}) and ascorbic acid, enabling the measurements in real clinical samples. We firstly prepared fluorescent graphdiyne oxide quantum dots (GDYO-QDs) with a facile ultrasonic protocol and characterized them with a range of techniques, showing a strong blue-green emission with 14.6% quantum yield. And it can be quenched efficiently by Fe^{3+} and recovered by ascorbic acid (AA). We have fabricated a Off/On fluorescent nanosensors based on the unique property. Our nanosensors are able to detect Fe^{3+} as low as 95 nmol L^{-1} with a promising dynamic range from 0.25 to 200 μmol L^{-1}. The LOD of AA was 2.5μmol L^{-1}, with range of 10-500 μmol L^{-1}. It showed a promising capability to detect Fe^{3+} and AA in serum samples compared to refereed technique.

Key words: fluorescence, quenching, graphdiyne, quantum dots, Fe^{3+}, ascorbic acid

1. Introduction

As one of the most trace metal elements in human bodies, iron (Fe) is the core part of hemoglobin and plays an important role in transporting oxygen and participating in human metabolism. [1-5] However, abnormal Fe^{3+} fluctuation is hazardous to human bodies, which can cause diseases, such as anemia, hepatitis, intelligence decline, agitans paralysis, and cancer. [6-8] Therefore, the monitoring of Fe^{3+} content is always an active issue in biosensing. Plenty of methods can be used to detect the above substances, such as mass spectroscopy [9], electrochemistry [10], colorimetric analysis [11, 12], amperometry [13] and florescence spectroscopy analysis [14-16]. Among them, fluorescence spectroscopy is a favorite method because of its simplicity, rapid response, and high sensitivity. [17, 18] Therefore, plenty of fluorescent sensors have been developed for Fe^{3+} detection. [19-21]

Quantum dots (QDs) are important materials in fluorescent sensors, due to their high stability, easy surface bioconjugation, and adaptable photophysical properties. [22] Traditional semiconductor QDs, including CdSe, PbS, CdS, are toxic for bioassay especially for in vivo applications due to the risk of leakage of heavy metal elements. [23, 24] Carbon-based QDs have inspired extensive interest because of their excellent optical property, low toxicity, chemical inertia and good biocompatibility. [25, 26] The representative carbon-based QDs, graphene QDs (GQDs) and carbon dots (CDs), have been widely used in fluorescent sensors for metal ions (such as Fe^{3+}, Cu^{2+}, Hg^{2+}), [21, 27, 28] the detection is influenced by the aspects of internal structure, surface state, and doping elements. [29] For Fe^{3+} detection, the effective strategy is N or S doping, [30, 31] which complicate the preparation of carbon-based QDs. Furthermore, the doping of heteroatoms such as N and S will increase the affinity of carbon-based QDs sensors to many other metal ions, which leading the low selectivity. The development of new type of carbon-based QDs without doping N or S may improve the selectivity.

Graphdiyne (GDY) is a new two-dimensional carbon nanomaterial comprising sp^2- and sp-hybridized carbon atoms with high π-conjugation. It has large triangular rings composed of 18 carbon atoms, which forms uniformly distributed pores. [32] All of

these special characteristics makes it unique electronic, optical, and electrochemical properties, which have been utilized as sensor materials. [33, 34] Due to its large π-conjugated surface, Li's group first reported GDY nanosheets as fluorescence quencher for DNA detection. [33] Wang's group also successfully applied GDY nanosheets for real-time fluorescence detection of DNA based on similar principle. [35] Wang developed a GDY based photoelectrochemical sensor, in which graphdiyne oxide nanosheets worked as signal inhibitor due to their unique electronic structure. [34] To the best of our knowledge, no sensor has been reported based on the optical property of GDY itself.

GDY is a semiconductor and its band gap can be tuned in the range of 0.14-1.22 eV based on the manner of stacking and number of layers. [36] GDY processes an outstanding extinction coefficient in the near-infrared region, thus it was used as photothermal conversion agents and imaging for tumor diagnosis and therapy. [37] It is known that the fluorescence of semiconductor can be tuned by changing its size, especially when the size is smaller than or equal to 10 nm, i.e. quantum dots (QDs). [38] The synthesis and study the fluorescent property of GDY based QDs may supplement available carbon based fluorescent materials, yet only one work reported graphdiyne oxide quantum dots (GDYO-QDs), they were used for bio-imaging. [39] The presence of triple bonds and large triangular rings facilitate the coordination with metal ions. [11] This may change the surface state or electronic structure of GDYO-QDs, leading the variation of their fluorescent property.

Based on the above assumption, we here report the synthesis GDYO-QDs using ultrasonic method firstly. Their fluorescence was quenched by the addition of Fe^{3+}, and the fluorescence was recovered by AA due to the reduction of Fe^{3+} to Fe^{2+}. Thus, an off/on sensor for Fe^{3+} and AA detection was established, as illustrated in Fig. 1. The detection condition optimization, sensitivity, and selectivity were investigated. The mechanism was proposed. Finally, GDYO-QDs were successfully applied to the quantitative determination of Fe^{3+} and AA in human serum. Our work provides a new carbon based QDs as optical sensor for Fe^{3+} and AA detection, it exhibited an excellent analytical performance.

< Fig. 1.>

2. Experimental Section

2.1. Materials and Methods.

Ascorbic acid, $Fe(NO_3)_3$, $MnCl_2$, $CaCl_2$, $Ni(NO_3)_2$,NaCl, CuCl2, $Zn(NO_3)_2$, $CdCl_2$, $PbCl_2$, NaOH, HCl and Phosphoric acid were purchased from Sinopharmaceutical Group Chemical Reagent Co., Ltd. THF and TBAF were purchased from Aladin Ltd. All reagents and solvents were purchased without further purification. Ultrapure water was used in the whole experiment. Fluorescent emission (FL) spectra were recorded on a Hitachi F-4600 luminescence spectrometer (Hitachi High-Tech Co., Ltd.). Fourier transform infrared (FT-IR) spectra (4000 - 400 cm^{-1}) were recorded on a Magna-560 spectrometer (Nicolet, Madison, WI). The transmission electron microscope (TEM) images were obtained from a JEOL-2010F microscope (Japan). The atomic force microscope (AFM) was performed using mica as the analytical substrate by Auto-probe CP Research (Thermo company, US). UV−vis spectra were collected on a TU-1900 spectrophotometer. X-ray photoelectron spectroscopy (XPS) was measured on a Thermo ESCALAB VG Science 250 spectrometer with monochromatic Al Kα excitation. The Raman spectra were analyzed by T64000 of HORIBA Scientific Company.

2.2. Materials Synthesis.

Firstly, the copper sheet is washed with HCl (4 M) and washed with water and ethanol under ultrasound. The copper sheet and pyridine (60 mL) were put into a three-port flask and heated at 120 ℃ for 1 h under the protection of N_2. Under the condition of ice bath, hexaethynylbenzene (200 mg) was dissolved in tetrahydrofuran (THF) of 50 mL, and 30 minutes was purged with nitrogen. 1 M TBAF was added to tetrahydrofuran (2.5 mL) and stirred at low temperature in nitrogen for 15 minutes. The reaction mixture was diluted with ethyl acetate, washed with saturated NaCl for 3 times, dried and filtered. The dried hexaethynylbenzene precursor was dissolved in pyridine (50 mL), transferred to a constant addition funnel protected by N_2, and dripped into the mixture containing pyridine (60 mL) and copper sheet at 80 °C. The addition process lasted for

10 hours. After adding the deprotected compound, the reaction mixture was kept at 120 °C for 3 days. After the reaction is completed, it is freeze-dried to evaporate pyridine. The crust products were collected by centrifugation, washed successively with hot DMF (80 °C) and ethanol (70 °C), and dried to obtain GDY. [32] Graphdiyne oxide (GDYO) was synthesized by acid-oxidation treatment. Briefly, GDY powder (10 mg) was first mixed with concentrated H_2SO_4 (98%, 2.5 mL) and hydrogen peroxide (30%, 1.0 mL). Then, the mixture was stirred in an ice-water bath for 1 hour. After centrifugation (8000 rpm, 10 min) and washing with ultra-pure water, the obtained suspension was freeze-dried to obtain GDYO.[40] GDYO-QDs were obtained by treating GDYO aqueous suspension (10 mL, 0.5 mg/mL) with ultrasonic (120 W, 30 kHz) for 24 hours. The obtained solution was heated by oil bath (100 ^{o}C, 6h), then centrifuged to get the supernatant, and GDYO-QDs were obtained.

2.3. Determination of Fe^{3+} and AA.

The fluorescence quenching of GDYO-QDs was carried out by Fe^{3+} at room temperature. In a typical operation, 200 μL of GDYO-QD (0.1mg mL^{-1}) solution was added to a Britton-Robinson (B−R) buffer solution (0.1mol L^{-1}, pH = 6.0). Different concentrations of Fe^{3+} solution and other metal ion solutions were freshly prepared before use. And the final volume of the mixture was 2.0 mL. For Fe^{3+} detection, different concentration of Fe^{3+} was added to the B−R buffer containing the same amount of GDYO-QDs, and the mixed solution was standing at room temperature for 20 minutes before spectral measurement. For AA detection, 200 μL GDYO-QDs (0.1mg mL^{-1}) and 200 μL of Fe^{3+} (2 mmol L^{-1}) were added the B−R buffer (0.1 mol L^{-1}, pH = 6.0). Consequently, different concentrations of AA solutions were added to the above mixture. The final volume of above mixture was 2.0 mL. The FL spectrum was recorded by fluorescence spectrophotometer at room temperature, and the excitation wavelength was 331 nm.

2.4. Detection of Fe^{3+} and AA in real sample.

Briefly, the treatment of human serum samples each serum sample was transferred to a cylindrical centrifuge tube, adding the same amount of ultra-pure water for swirling

mixing, and centrifuged 10 minutes at the speed of 6000 rpm. Then, remove the aluminum cover and transfer the clarified supernatant to the glass bottle for use in the next test. In order to determine Fe^{3+} in serum samples, the treated human serum was added to GDYO-QDs solution. In addition, Serum sample 1 was further added with Fe^{3+} concentration of 50, 100, 150 μmol L^{-1}, respectively. It was used to explore the recovery rates. The serum sample detection of Fe^{3+} was done with adding GDYO-QDs and Fe^{3+} after placing it for 20 minutes. At the same time, we also applied the sensor to the analysis of AA in human serum. Human serum samples were added to GDYO-QDs/Fe^{3+} (200 μmol L^{-1}) solution. Then mixed with different concentrations of AA (50, 200, 400 μmol L^{-1}). The serum sample detection of AA was done with adding GDYO-QDs after placing it for 3 minutes. All the above tests were tested at room temperature.

3. Results and discussion

3.1. Characterization of GDY and GDYO-QDs.

< Fig. 2.>

In this work, GDY was prepared by cross-coupling reaction of hexaethynylbenzene precursor on copper surface, and GDY powder was oxidized by the strong oxidation. GDYO-QDs was further prepared by physical ultrasonic crushing. The morphologies of the as-prepared GDYO-QDs were characterized by TEM, as shown in Fig. 2a. Their diameters were 4.45±2 nm (by judging from image analyses of 100 individual particles). Fig. 2b shows the HRTEM images of GDYO-QDs, they clearly reveal a good crystallinity of GDYO-QDs with a layer spacing of 0.36 nm, which is in agreement with the interlayer spacing of GDY. [41] AFM image shows the typical topographic height of GDYO-QDs is in the range of 3-4 nm (Fig. 2c). The result is significantly confirmed by images of naked substrates (Fig. S1). The zeta potential of GDYO-QDs is -35.1 mV (Fig. S2), which is due to the presence of abundant hydrophilic groups (hydroxyl and carboxyl groups). The triple bonds in GDYO-QDs were determined by Raman spectroscopy. Fig. 2d shows the peaks at 1382 and 1598 cm^{-1} correspond to the

D band and G band of GDY, GDYO and GDYO-QDs, respectively. The I_D/I_G values of them were 0.867, 0.896 and 0.935, respectively. The increasing value of I_D/I_G indicates that the defects increases with the oxidation process of GDY. Two weak peaks at 1919 and 2188 cm^{-1} were attributed to the vibration of conjugated diyne links (−C≡C−C≡C−), which is in agreement with the previous report.[42] It proves that GDYO-QDs have a carbon skeleton similar to that of GDY and GDYO (Fig. 2d).

The atomic ratio of O/C in carbon materials plays an important role in their properties including heterogeneous electron transfer, chemical adsorption. [43, 44] Thus, X-ray photoelectron spectroscopy (XPS) analysis was used to illustrate the O/C ratios during the preparation of GDYO-QDs (Fig. 2e, f and Fig. S3). As shown in Table S1, the O/C ratio of GDYO-QDs (46.13 %) was higher than GDY (26.93%), indicating that the ultrasonic crushing process virtually led to the generation of oxygen-containing species, it is in agreement with the FT-IR results (Fig. S4). The C1s spectrum of GDYO-QDs and GDY can be deconvoluted into C−C (sp^2), C-C (sp), C−O, and C=O at binding energies of 284.5, 285.2, 285.9, and 288.2 eV, respectively (Fig. 2e, f), which suggesting the similar carbon skeletons they have. Compared with GDY, the intensity of the peak at 284.5 eV (sp^2 - hybridized carbon) strengthened, while the peak at 285.2 eV (sp-hybridized carbon) obviously decreased, as shown in Fig. 2e. These results showed the partial oxidation of GDY and a certain percentage of the carbon triple bonds was broken during preparation of the GDYO-QDs. Moreover, a decrease of the C=O content and an increase of the C−O content in surface groups indicate the carboxylates were possibly reduced into lactones or ethers. [42] The O1s spectrum of GDY, GDYO and GDYO-QDs to confirm the hypothesis. (Fig. S5)

3.2 Optical properties of GDYO-QDs.

< Fig. 3.>

Fig. 3a and Fig. S6 show the absorption band of GDY, GDYO and GDYO-QDs decreased from 200 nm to 800 nm, an insignificant absorption band at ca. 330 nm was observed in the spectra of GDYO-QDs, which is attributed to n−π* transitions of

conjugated domains of GDYO-QDs. [48] The fluorescence quantum yield of GDYO-QDs was calculated to be 14.6%, the calculation is shown in Supporting Information. Fig. 3b shows the maximum emission was observed at 446 nm when the excitation wavelength was 331 nm. In 3D image (Fig. 3c), it shows the change of fluorescence intensity of GDYO- QDs under different excitation wavelengths (z axis: 280-380 nm) and emission wavelengths (x axis: 350-540 nm). The positions of the excitation and emission peaks of GDYO-QDs confirm that the optimal excitation and emission wavelengths are about 330 and 450 nm, respectively. The emission spectrum of GDYO-QDs was recorded step by step in the excitation range from 301 to 371 nm with an increment of 10 nm (Fig. 3d). The emission peak red-shifted gradually with the increase of excitation wavelength. This phenomenon is due to the size-dependent band gap of GDYO-QDs and the existence of various surface defect states or different emission traps. [46] Fig. 3e shows the change of fluorescence intensity of GDYO-QDs in different concentrations of salt solution, indicating that it can tolerate high salt concentrations. By comparing the fluorescence properties of GDYO- QDs prepared in three different batches (Fig.S7), the small difference indicates that the preparation process is relatively stable. In addition, the change of fluorescence intensity of GDYO-QDs in 14 days was studied, and it was found that the quantum dots could still maintain good fluorescence properties after being stored for a long time (Fig.S8). Fig. 3f shows the fluorescence intensity of GDYO-QDs changed very little after 1 hour of continuous UV irradiation, indicating an excellent resistance to photobleaching of GDYO-QDs.

3.3. Analytical performance for Fe^{3+} and AA detection under optimized condition.

< Fig. 4.>

A fluorescence sensor based GDYO-QDs were established for Fe^{3+} and AA detection. The experimental conditions including the pH value of the assay and the reaction time were investigated and optimized, as elaborated in Supporting Information (Fig.9-12). Fig. 4a shows the fluorescence spectra of GDYO-QDs solution with the addition of different Fe^{3+} concentrations. The fluorescence intensity of GDYO-QDs at 446 nm

decreased with the increase of Fe^{3+} concentration. The curves of quenching ratio (F_0 - F)/F and Fe^{3+} concentration from 0 to 300 μmol L^{-1} were performed (Fig. 4b), where F_0 and F are the fluorescence intensity of GDYO-QDs solution before and after the addition of Fe^{3+}, respectively. The limit of detection (LOD) was 95 nmol L^{-1} (S/N = 3, R^2 = 0.9889), with a linear range of 0.25-200 μmol L^{-1} was obtained. LOD is much lower than the Environmental Protection Agency (US EPA) guideline (5.37 μmol L^{-1}) in biological serum and the linear range meets the needs of detection in our daily life. A comparison of different QD based fluorescent sensors for Fe^{3+} detection is summarized in Table S2; our sensor was much sensitive than most of the other fluorescent sensors.

AA was used to recover the fluorescence intensity of GDYO-QDs, because of AA can reduce Fe^{3+} to Fe^{2+} (Fig. 4c). Notably, AA had no effect on the fluorescence intensity of GDYO-QDs when without Fe^{3+} (Fig. S13). The fluorescence recovery tended to be stable with the addition of AA after 4 minutes (Fig. S14). With the increase of AA concentration, the fluorescence of GDYO-QDs at 446 nm recovered gradually, the fluorescence recovery rate was about 85%. The LOD was 2.5 μmol L^{-1} (S/N = 3, R^2 = 0.9906), with a linear range of 10-500 μmol L^{-1} (Fig. 4d). In addition, the reversible fluorescence change of GDYO-QDs after adding AA in the presence of Fe^{3+} was also investigated, as shown in Figure S12. The fluorescence intensity of GDYO-QDs was quenched rapidly after the addition of Fe^{3+}. After adding AA, the fluorescence intensity of GDYO-QDs was recovered within 2 min (Fig. S15), and there was a good recovery in three consecutive cycles. The results showed that the system was reversible and could be recycled for at least 3 times for simultaneous determination of Fe^{3+} and AA.

The selectivity of the sensor was investigated, two groups of control experiments were carried out. Firstly, 100 μmol L^{-1} (Fig. 4e) and 1000 μmol L^{-1} (Fig. S16) of biological and environment-related metal ions were added to the GDYO-QDs solution, including Fe^{3+}, Fe^{2+}, Cu^{2+}, Mn^{2+}, Cr^{3+}, Cd^{2+}, Ca^{2+}, Mg^{2+}, Na^{+}, Ni^{2+}, Pb^{2+}, Al^{3+}, Zn^{2+} and the mixed solution of various metal ions, the fluorescence intensity changes were recorded. Obviously, it can be seen that the quenching effect of Fe^{3+} on GDYO-QDs reached more than 80 %, which shows a good selectivity for Fe^{3+}. Moreover, the

selectivity of GDYO QDs for AA over other interference substances (L-Threonine (L-Thr), Glutamic acid (Glu), Carbonic Anhydrase (CA), Homocysteine (Hcy), Glutathione (GSH), Proline (Pro), L-Valine (L-Val), L-Cysteine (L-Cys), L-Alanine (L-Ala), DL- Phenylalanine (DL-Phe), Uric acid (UA) , Dopamine (DA)) was also investigated, as shown in Fig. 4f. The result shows that the fluorescence recovery of GDYO-QDs/Fe^{3+} sensor by AA is much higher than that of other interfering substances. At the same time, in the presence of metal ions and other interfering organic compounds, the fluorescence of the system changed slightly, which shows high selectivity for Fe^{3+} and AA (Fig. S17). In other words, our sensor shows a high anti-interference capability.

3.4. Mechanism of fluorescence quenching by Fe^{3+}.

< Fig. 5.>

On the basis of previous reports, the quenching effect is mainly attributed to the action of inner filter effect (IFE) or photoinduced electron transfer (PET). [3, 47] To further verify this hypothesis, the reaction process of GDYO-QDs with Fe^{3+} in the aspects of IFE and PET was investigated. In order to verify the mechanism of IFE, we firstly studied the optical properties of GDYO-QDs and Fe^{3+}. It can be seen from Fig. 5a that Fe^{3+} has a strong absorption in the range of 260-400 nm, overlapping with the excitation band of GDYO-QDs (331 nm), which leads to the formation of IFE between GDYO-QDs and Fe^{3+}. [3, 48] Fig. 5b shows the time-resolved fluorescence decay spectra of GDYO-QDs with 0, 50 and 100 μmol L^{-1} of Fe^{3+}, a double exponential decay function recorded the fluorescence decay time. The fluorescence decay time of GDYO-QDs is 10.22 ns without Fe^{3+}. After adding Fe^{3+}, whose concentrations were 50 and 100 μmol L^{-1}, the corresponding decay time were 10.36 and 10.47 ns, respectively. The fluorescence decay time changed insignificantly after the addition of Fe^{3+}, indicating quenching mechanism is not only due to IFE, because IFE is a static quenching process that does not cause disturbance of excited states of fluorophores. [49, 50] We made an additional study on the effect of IFE on the quenching process, according to absorption

characteristics and the cuvette geometry (Fig. 5c), the IFE on GDYO-QDs and Fe^{3+} was corrected by the following equation. [51]

$$CF = \frac{F_{cor}}{F_{obsd}} = \frac{2.3dA_{ex}}{1 - 10^{-dA_{ex}}} \times \ 10^{gA_{em}} \times [2.3sA_{em}/(1 - 10^{-sA_{em}})]$$

Where, CF is the corrected factor; F_{cor} and F_{obsd} severally represent the corrected fluorescence intensity by removing IFE from F_{obsd} and the observed fluorescence intensity of GDYO-QDs. A_{ex} and A_{em} represent the absorbance per centimeter of GDYO- QDs at the excitation wavelength and the emission wavelength, respectively. Fig. 5c shows the quenching efficiency of observed (Q_{obsd}) and corrected (Q_{cor}) fluorescence of GDYO-QDs at different concentrations of Fe^{3+}. Table S3 summarizes the detailed calculation process and results. From the above results show a 35% of quenching efficiency of Fe^{3+} to GDYO-QDs can be obtained via IFE, which indicates the quenching of GDYO-QDs by Fe^{3+} was not completely dependent on IFE.

To verify the mechanism of PET, the electron bandgap (Eg) and valence band (VB) of GDYO-QDs were studied (Fig. 5d, e). By using the Tauc plot (Fig. 5d) in UV-Vis absorption spectrum (Fig. 3a), the direct electron band gap of GDYO-QDs was 1.65 eV. Through the XPS valence band spectrum (Fig. 5e), the VB of GDYO-QDs was calculated to be 2.01 eV (EVB) vs Normal Hydrogen Electrode (NHE). According to the formula: $E_{CB} = E_{VB} - E_g$, the conduction band (CB) is 0.36 eV vs NHE. While the standard electrode potential of Fe^{3+} / Fe^{2+} is 0.77 eV vs NHE, which is located between VB and CB of GDYO- QDs. When light excites the GDYO-QDs, the electrons of VB are excited to CB; consequently, these electrons transfer to the d-orbit of Fe^{3+} instead of going back to VB, thus fluorescence quenching is caused by PET process, as illustrated in Fig. 5f. [52, 53] In summary, the fluorescence quenching of GDYO-quantum dots by Fe^{3+} is caused by the synergistic effect of IFE and PET.

3.5. Real application of GDYO-QDs for analysis of Fe^{3+} and AA in fetal bovine serum samples.

The potential of biological application was carried out by analyzing Fe^{3+} in human

serum samples. Since the concentrations of Mg^{2+} and Ca^{2+} are usually 100 times higher than Fe^{3+} in human serum samples, we firstly studied the selectivity of the assay towards Fe^{3+} in the presence of Mg^{2+} (10 mmol L^{-1}) and Ca^{2+} (10 mmol L^{-1}). The results indicated no obvious effect was caused by Mg^{2+} and Ca^{2+} on the fluorescence intensity of GDYO-QDs (Fig. S18). In order to verify the accuracy of this method, atomic absorption spectrometry (AAS) was used as the standard method for the determination of Fe^{3+} in human serum. Table 1 shows the related recovery results of the above samples, which is in the range of 98.77% - 102.66%. At the same time, with the nitrate of Fe^{3+} as the standard solution, the unknown content of Fe^{3+} in human serum was determined by standard addition method. In addition, the detection and analysis of AA in fetal bovine serum was also carried out. GDYO-QDs of 200 μmol L^{-1} was added to fetal bovine serum as sample solution. Three different concentrations of AA (50, 200 and 400 μmol L^{-1}) added to the sample solution. As shown in Table S4, the recovery range of the relevant samples is 97.68% - 103.27%. The relative standard deviation (n = 3) is less than 4.21%. The good recovery rate shows the reliability of the assay, the low deviation proves that the sensor has the potential to be used in clinical detection.

< Table 1.>

4. Conclusions

GDYO-QDs were fabricated through acid-oxidation treatment and ultrasound method, their optical property was investigated. The fluorescence of GDYO-QDs can be quenched efficiently by Fe^{3+}, and can be recovered by AA, which can be utilized as a fluorescent sensor for Fe^{3+} and AA detection. The results showed a selective and sensitive sensor for Fe^{3+} and AA detection was obtained, the LOD is 95 nmol L^{-1}, with range of 0.25-200 μmol L^{-1}, (AA: LOD is 2.5μmol L^{-1}, with range of 10-500 μmol L^{-1}). In addition, this sensor was applied successfully for Fe^{3+} detection in fetal bovine serum sample. Finally, the quenching mechanism by Fe^{3+} was proposed as that the synergistic effect between IFE and PET. Our present study provides a newly carbon-based fluorescent sensor for rapid, highly selective, and sensitive detection of Fe^{3+} and AA.

In the present work, the quantum yield of GDYO-QDs is not high, which limits the sensitivity of detection, further work will be focused on the improvement of their quantum yield.

Acknowledgements

This work was financially supported by the National Natural Science Foundation of China (21501106), the Scientific Research Foundation for the Returned Overseas Chinese Scholars and Qingdao Municipal Science and Technology Commission (16-5-1-86-jch, 19-6-2-73-cg), Chemistry Faculty Talents Foundation of Qingdao University of Science and Technology.

References

[1] A. Syal, D. Sud, Development of highly selective novel fluorescence quenching probe based on Bi_2S_3-TiO_2 nanoparticles for sensing the Fe(III), Sens. Actuators B-Chem. 266 (2018) 1-8.

[2] Kardar, Z. S., Shemirani, F., & Zadmard, R., Determination of iron (II) and iron (III) via static quenching of the fluorescence of tryptophan-protected copper nanoclusters, Microchim. Acta, 187 (2020) 1-9.

[3] X. Guo, G. Yue, J. Huang, C. Liu, Q. Zeng, L. Wang, Label-Free Simultaneous Analysis of Fe(III) and Ascorbic Acid Using Fluorescence Switching of Ultrathin Graphitic Carbon Nitride Nanosheets, Acs Applied Materials & Interfaces. 10 (2018) 26118-26127.

[4] Cao H , Chen Z , Zheng H , et al. Copper nanoclusters as a highly sensitive and selective fluorescence sensor for ferric ions in serum and living cells by imaging[J], Biosensors & Bioelectronics. 62 (2014) 189-195.

[5]Aptasensor Based on MoS_2 Quantum Dots with Upconversion Fluorescence for Microcystin-LR Detection via the Inner Filter Effect[J], ACS Sustainable Chemistry And Engineering. 8(2020) 29:10939-10946.

[6] G.T. Sucak, Z.A. Yegin, Z.N. zkurt, Z. Ak, T. Karakan, G.J.B.M.T. Akyol, The role of liver biopsy in the workup of liver dysfunction late after SCT: is the role of iron overload underestimated?, Bone Marrow Transplant. 42 (2008) 461-467.

[7] Weinstein, D.A., Inappropriate expression of hepcidin is associated with iron refractory anemia: implications for the anemia of chronic disease, Blood. 100 (2002) 3776-3781.

[8] N. Narayanaswamy, T.J.S. Govindaraju, Aldazine-based colorimetric sensors for Cu^{2+} and Fe^{3+}, Sens. Actuators B-Chem 161 (2012) 304-310.

[9] A. Spolaor, P. Vallelonga, J. Gabrieli, G. Cozzi, C. Boutron, C. Barbante, Determination of Fe^{2+} and Fe^{3+} species by FIA-CRC-ICP-MS in Antarctic ice samples, J. Anal. At. Spectrom. 27 (2012) 310-317.

[10] A. Bobrowski, K. Nowak, J. Zarębski, Application of a bismuth film electrode to the voltammetric determination of trace iron using a Fe(III) – TEA – BrO3−catalytic system, Anal. Chem. 382 (2005) 1691-1697.

[11] Liang, C. , Lan, Y. , Sun, Z. , Zhou, L. , Qin, X., Synthesis of carbon quantum dots with iron and nitrogen from passiflora edulis and their peroxidase-mimicking activity for colorimetric determination of uric acid. Microchim. Acta, 187(2020).

[12] N. Sui, F. Liu, K. Wang, F. Xie, L. Wang, J. Tang, M. Liu, W.W. Yu, Nano Au-Hg amalgam for Hg^{2+} and H_2O_2 detection, Sens. Actuators B-Chem. 252 (2017) 1010-1015.

[13] A. Umar, M.S. Chauhan, S. Chauhan, R. Kumar, P. Sharma, K.J. Tomar, R. Wahab, A. Al-Hajry, D. Singh, Applications of ZnO nanoflowers as antimicrobial agents for Escherichia coli and enzyme-free glucose sensor, J Biomed Nano. 9 (2013) 1794-1802.

[14] L. Long, L. Zhou, L. Wang, S. Meng, A. Gong, C. Zhang, A ratiometric fluorescent probe for iron(III) and its application for detection of iron(III) in human blood serum, Anal Chim Acta. 812 (2014) 145-151.

[15] M. Cacciari, M.L. Mangano, P. Nason, Gluon PDF constraints from the ratio of forward heavy-quark production at the LHC at $\sqrt{s}$ = 2 and 13 TeV, Eur Phys J C Part Fields. 75 (2015) 610.

[16] L. Qiu, C. Zhu, H. Chen, M. Hu, W. He, Z. Guo, A turn-on fluorescent Fe(III) sensor derived from an anthracene-bearing bisdiene macrocycle and its intracellular imaging application, Chem Commun (Camb). 50 (2014) 4631-4634.

[17] Omer K M, Hassan A Q. Chelation-enhanced fluorescence of phosphorus doped carbon nanodots for multi-ion detection, Microchim. Acta, 184 (2017) 2063-2071.

[18] Xiao, Hailian, Wang, Lina, Xie, Fengxia, Yu, William, W., S.J.M.A.A.I.J.f. Physical, C.M.o. Analysis, Ultrasensitive aptamer-based thrombin assay based on metal enhanced fluorescence resonance energy transfer, Microchim. Acta. 183 (2016) 1563-1570.

[19] B. Shi, Y. Su, L.L. Zhang, M. Huang, R. Liu, S.J. Zhao , Nitrogen and Phosphorus Co-doped Carbon Nanodots as a Novel Fluorescent Probe for Highly Sensitive Detection of Fe^{3+} in Human Serum and Living Cells, Acs Applied Materials & Interfaces. 8 (2016) 10717-10725.

[20] J. Shangguan, J. Huang, D. He, X. He, K. Wang, R. Ye, X. Yang, T. Qing, J. Tang, Highly Fe(III)-Selective Fluorescent Nanoprobe Based on Ultrabright N/P Codoped Carbon Dots and Its Application in Biological Samples, Anal Chem. 89 (2017) 7477-7484.

[21] S. Li, Y. Li, J. Cao, J. Zhu, L. Fan, X. Li, Sulfur-doped graphene quantum dots as a novel fluorescent probe for highly selective and sensitive detection of Fe(III), Anal Chem. 86 (2014) 10201-10207.

[22] K.D. Wegner, N.J. Hildebrandt, Quantum dots: bright and versatile in vitro and in vivo fluorescence imaging biosensors, Chem. Soc. Rev. 44 (2015) 4792-4834.

[23] P. Zuo, X. Lu, Z. Sun, Y. Guo, H. He, A review on syntheses, properties, characterization and bioanalytical applications of fluorescent carbon dots, Microchim. Acta 183 (2015) 519-542.

[24] R. Liu, D. Wu, S. Liu, K. Koynov, W. Knoll, Q. Li, An aqueous route to multicolor photoluminescent carbon dots using silica spheres as carriers, Angew Chem Int Ed Engl. 48 (2009) 4598-4601.

[25] S.N. Baker, G.A. Baker, Lumineszierende Kohlenstoff-Nanopunkte: Nanolichtquellen mit Zukunft, Angewandte Chemie. 122 (2010) 6876-6896.

[26] S. Xu, et al. Lysosome-targeted ratiometric fluorescent sensor for monitoring pH in living cells based on one-pot-synthesized carbon dots, Microchimica Acta 187 (2020) 1-9.

[27] S. Xu, Y. Liu, H. Yang, K. Zhao, J. Li, A.J. Deng, Fluorescent nitrogen and sulfur co-doped carbon dots from casein and their applications for sensitive detection of Hg $^{2+}$ and biothiols and cellular imaging, Anal. Chim Acta. 964 (2017) 150-160.

[28] Omer, K. M. , Hassan, A. Q., Chelation-enhanced fluorescence of phosphorus doped carbon nanodots for multi-ion detection. Microchim. Acta, 184 (2017) 2063-2071.

[29] Y.L. Zhang, L. Wang, H.C. Zhang, Y. Liu, S.T.J. Lee, Graphitic carbon quantum dots as a fluorescent sensing platform for highly efficient detection of Fe^{3+} ions, Rsc Advances. 3 (2013) 3733-3738.

[30] C. Sun, Y. Zhang, P. Wang, Y. Yang, Y. Wang, J. Xu, Y. Wang, W.W.J. Yu, Synthesis of Nitrogen and Sulfur Co-doped Carbon Dots from Garlic for Selective Detection of Fe^{3+}, Nanoscale Res Lett. 11 (2016) 110.

[31] Y. Liang, L. Xu, K. Tang, Y. Guan, T. Wang, H. Wang, W.W. Yu, Nitrogen-doped carbon dots used as an “on–off–on” fluorescent sensor for Fe^{3+} and glutathione detection, Dyes and Pigments. 178 (2020) 178:108358.

[32] G. Li, Y. Li, H. Liu, Y. Guo, Y. Li, D. Zhu, Architecture of graphdiyne nanoscale films, Chem Commun (Camb). 46 (2010) 3256-3258.

[33] C. Wang, P. Yu, S. Guo, L. Mao, H. Liu, Y. Li, Graphdiyne oxide as a platform for fluorescence sensing, Chem Commun (Camb). 52 (2016) 5629-5632.

[34] H. Wang, K. Deng, J. Xiao, C. Li, S. Zhang, X. Li, A sandwich-type photoelectrochemical sensor based on tremella-like graphdiyne as photoelectrochemical platform and graphdiyne oxide nanosheets as signal inhibitor, Sens. Actuators B-Chem. 304 (2020).

[35] N. Parvin, Q. Jin, Y. Wei, R. Yu, B. Zheng, L. Huang, Y. Zhang, L. Wang, H. Zhang, M.J. Gao, Few-Layer Graphdiyne Nanosheets Applied for Multiplexed Real-Time DNA Detection, Adv. Mater. 29 (2017) 1606755.1606751-1606755.1606757.

[36] M. Long, L. Tang, D. Wang, Y. Li, Z.J. Shuai, Electronic Structure and Carrier Mobility in Graphdiyne Sheet and Nanoribbons: Theoretical Predictions, Acs Nano. 5 (2011) 2593-2600.

[37] J. Jin, M. Guo, J. Liu, J. Liu, H. Zhou, J. Li, L. Wang, H. Liu, Y. Li, Y.J. Zhao, Interfaces, Graphdiyne Nanosheet-Based Drug Delivery Platform for Photothermal/Chemo-therapy Combination Treatment of Cancer, Acs Appl. Mater. Interfaces. (2018) acsami.7b17219.

[38] W.W. Yu, Y.A. Wang, X.J. Peng, Formation and Stability of Size-, Shape-, and Structure-Controlled CdTe Nanocrystals: Ligand Effects on Monomers and Nanocrystals, Chem. Mater.15 (2003) 4300-4308.

[39] H. Min, Y. Qi, Y. Chen, Y. Zhang, G.N.J., Synthesis and Imaging of Biocompatible Graphdiyne Quantum Dots, Acs Appl. Mater. Interfaces. 11 (2019) 10.1021.

[40] Graphdiyne Oxides as Excellent Substrate for Electroless Deposition of Pd Clusters with High Catalytic Activity, J. Am. Chem. Soc. 137(2015) 16:5260–5263.

[41] P. Kuang, B. Zhu, Y. Li, H. Liu, J. Yu, K. Fan, Graphdiyne: a superior carbon additive to boost the activity of water oxidation catalysts, Nanoscale Horizons 3 (2018) 317-326.

[42] S. Guo, H. Yan, F. Wu, L. Zhao, P. Yu, H. Liu, Y. Li, L. Mao, Graphdiyne as Electrode Material: Tuning Electronic State and Surface Chemistry for Improved Electrode Reactivity, Anal Chem. 89 (2017) 13008-13015.

[43] V. Georgakilas, J.N. Tiwari, K.C. Kemp, J.A. Perman, A.B. Bourlinos, K.S. Kim, R.J.C.r. Zboril, Noncovalent functionalization of graphene and graphene oxide for energy materials, biosensing, catalytic, and biomedical applications, Chem. Rev. 116 (2016) 5464-5519.

[44] S. Ning, L. Wang, X. Wu, X. Li, S. Jing, H. Xiao, M. Liu, J. Wan, W.W.J. Yu, Polyethylenimine modified magnetic graphene oxide nanocomposites for Cu^{2+} removal, Rsc. Adv. 5 (2014) 746-752.

[45] A. Mewada, S. Pandey, S. Shinde, N. Mishra, G. Oza, M. Thakur, M. Sharon, M. Sharon, Green synthesis of biocompatible carbon dots using aqueous extract of Trapa bispinosa peel, Mater Sci Eng C Mater Biol Appl. 33 (2013) 2914-2917.

[46] J. Peng, W. Gao, B.K. Gupta, Z. Liu, R. Romero-Aburto, L. Ge, L. Song, L.B. Alemany, X. Zhan, G. Gao, S.A. Vithayathil, B.A. Kaipparettu, A.A. Marti, T. Hayashi,

J.J. Zhu, P.M. Ajayan, Graphene quantum dots derived from carbon fibers, Nano Lett. 12 (2012) 844-849.

[47] Y. Li, J. Cai, F. Liu, H. Yu, F. Lin, H. Yang, Y. Lin, S. Li, Highly crystalline graphitic carbon nitride quantum dots as a fluorescent probe for detection of Fe(III) via an innner filter effect, Microchim. Acta 185 (2018) 134.

[48] G.N. Kalantzopoulos, F. Lundvall, S. Checchia, A. Lind, D.S. Wragg, H. Fjellvag, B. Arstad, In Situ Flow MAS NMR Spectroscopy and Synchrotron PDF Analyses of the Local Response of the Bronsted Acidic Site in SAPO-34 during Hydration at Elevated Temperatures, Chemphyschem. 19 (2018) 519-528.

[49] W. Kong, D. Wu, L. Xia, X. Chen, G. Li, N. Qiu, G. Chen, Z. Sun, J. You, Y. Wu, Carbon dots for fluorescent detection of alpha-glucosidase activity using enzyme activated inner filter effect and its application to anti-diabetic drug discovery, Anal Chim Acta. 973 (2017) 91-99.

[50] X. Zhu, T. Zhao, Z. Nie, Y. Liu, S. Yao, Non-redox modulated fluorescence strategy for sensitive and selective ascorbic acid detection with highly photoluminescent nitrogen-doped carbon nanoparticles via solid-state synthesis, Anal Chem. 87 (2015) 8524-8530.

[51] S.J. Xiao, X.J. Zhao, P.P. Hu, Z.J. Chu, C.Z. Huang, L. Zhang, Highly Photoluminescent Molybdenum Oxide Quantum Dots: One-Pot Synthesis and Application in 2,4,6-Trinitrotoluene Determination, ACS Appl Mater Interfaces. 8 (2016) 8184-8191.

[52] L. Guo, Y. Liu, R. Kong, G. Chen, Z. Liu, F. Qu, L. Xia, W. Tan, A Metal-Organic Framework as Selectivity Regulator for Fe(III) and Ascorbic Acid Detection, Anal Chem. 91 (2019) 12453-12460.

[53] Y. Yan, C. Zhang, W. Gu, C. Ding, X. Li, Y. Xian, Facile Synthesis of Water-Soluble WS_2 Quantum Dots for Turn-On Fluorescent Measurement of Lipoic Acid, J. Phys. Chem. C. 120 (2016) 12170-12177.

Fig. 1. Synthesis of GDYO-QDs and fluorescent detection of Fe^{3+} and AA.

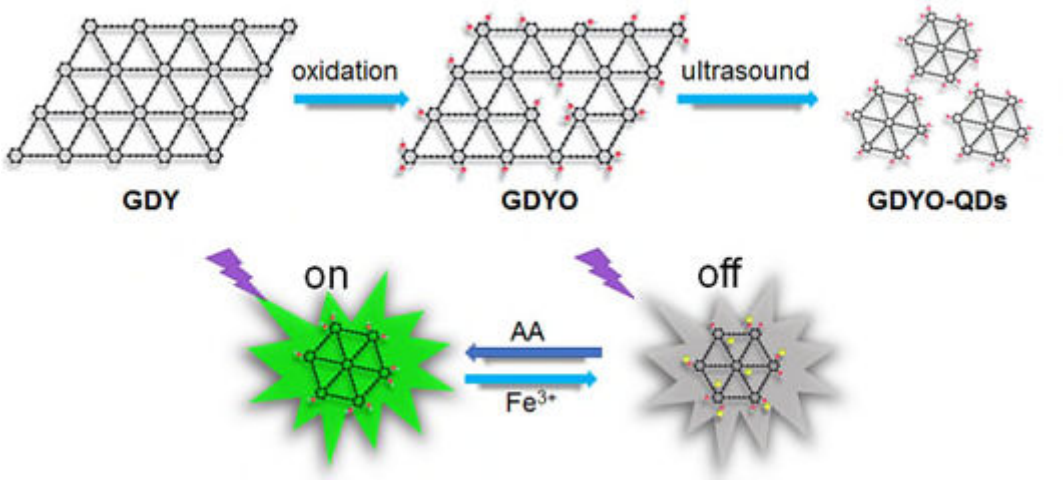

Fig. 2. (a) TEM image of GDYO-QDs. Inset: size distribution of GDYO-QDs. (b) High resolution TEM images of GDYO-QDs. (c) AFM images of GDYO-QDs. (d) Raman spectroscopy of GDY and GDYO-QDs. High-resolution C1s spectra of (e) GDY and (f) GDYO-QDs.

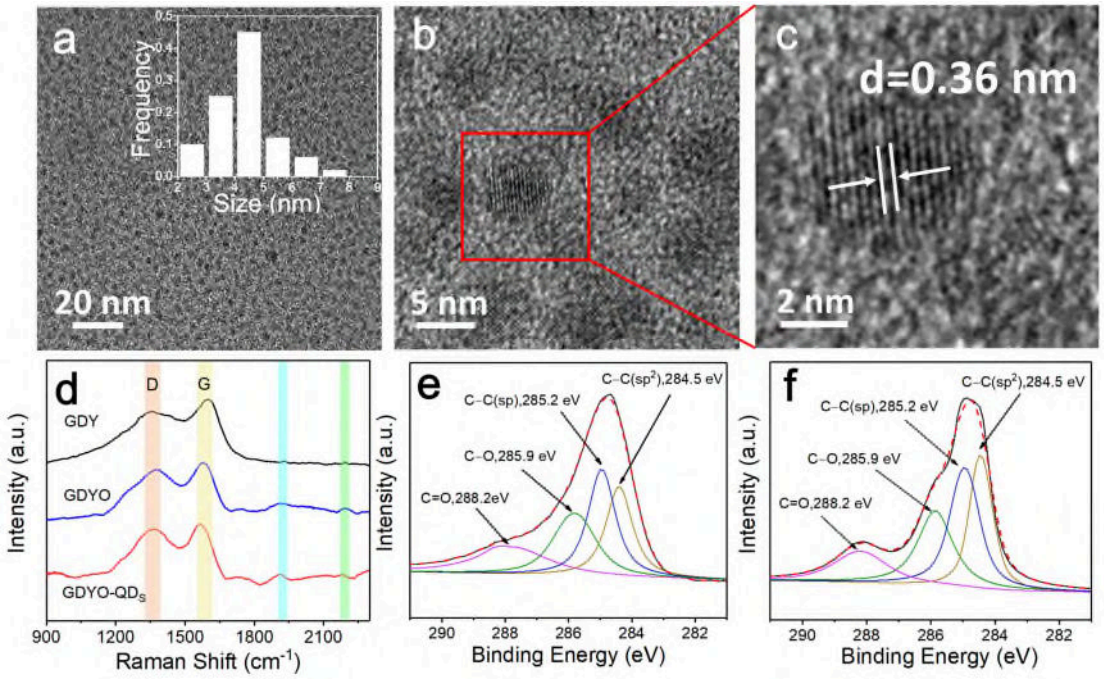

Fig 3. (a) UV−vis absorption spectra of GDY and GDYO-QDs. Inset: photographs of GDYO-QDs solution (dispersed in water) under sunlight (left) and under 360 nm UV irradiation (right). (b) Excitation and emission spectra of GDYO-QDs. (c) 3D fluorescence spectra of GDYO-QDs. (d) Fluorescence spectra of GDYO-QDs excited at different wavelengths. (e) Fluorescence intensity (at 446 nm) of GDYO-QDs influenced by different concentrations of salt solutions. (n=3) (f) Photo stability of GDYO-QDs under irradiation for 1 h.

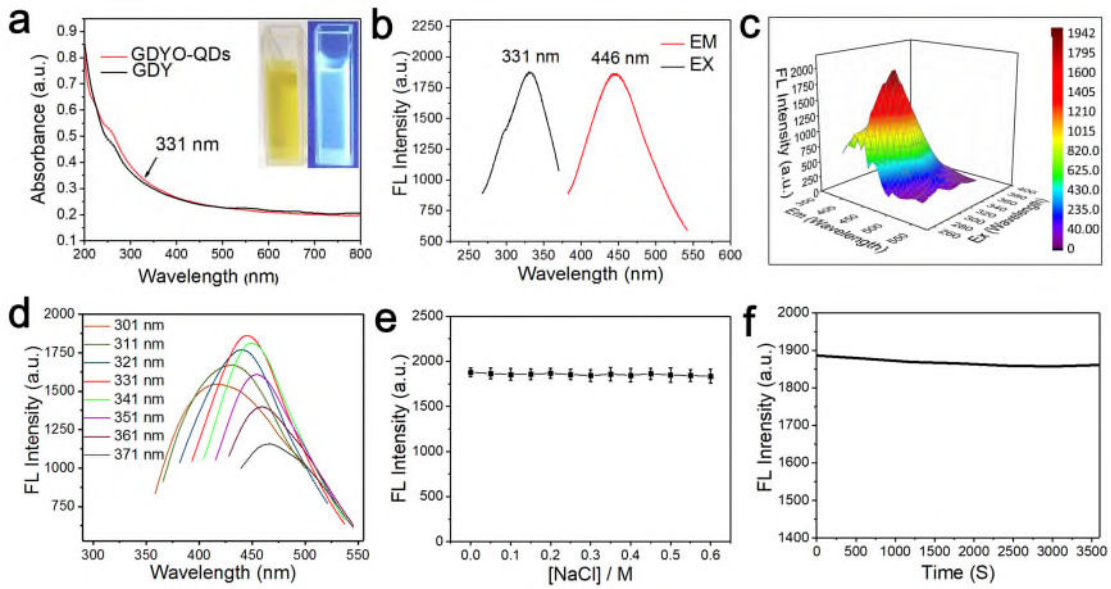

Fig. 4. (a) Fluorescence spectra of GDYO-QDs for the detection of different concentrations of Fe^{3+} (from top to bottom: 0 - 300 μmol L^{-1}). (b) Calibration curve of $(F_0 - F)/F$ versus Fe^{3+} concentration, the inset is the calibration curve of $(F_0 - F)/F$ and low concentration Fe^{3+} (0.25-200 μmol L^{-1}). (c) Fluorescence emission spectra of GDYO-QDs and Fe^{3+} (200 μmol L^{-1}) with different concentrations of AA (from bottom to top: 0 – 1000 nmol L^{-1}). (d) Calibration curve of $(F – F_0)/F_0$ versus concentration of AA, the inset is the calibration curve of $(F – F_0)/F_0$ versus concentration of AA and low concentration AA (10-500 μmol L^{-1}). (e) Selective response of aqueous GDYO-QDs towards different metal ions (the concentrations of metal ions were all 50 μmol L^{-1}), (f) Selective response of aqueous GDYO-QDs towards other interference substances. (concentrations of AA and interference substances were all 400 μmol L^{-1}), (λex = 331 nm). F_0 and F are the fluorescence intensities of GDYO-QDs at 446 nm in the absence and presence of Fe^{3+}, respectively. (n=3)

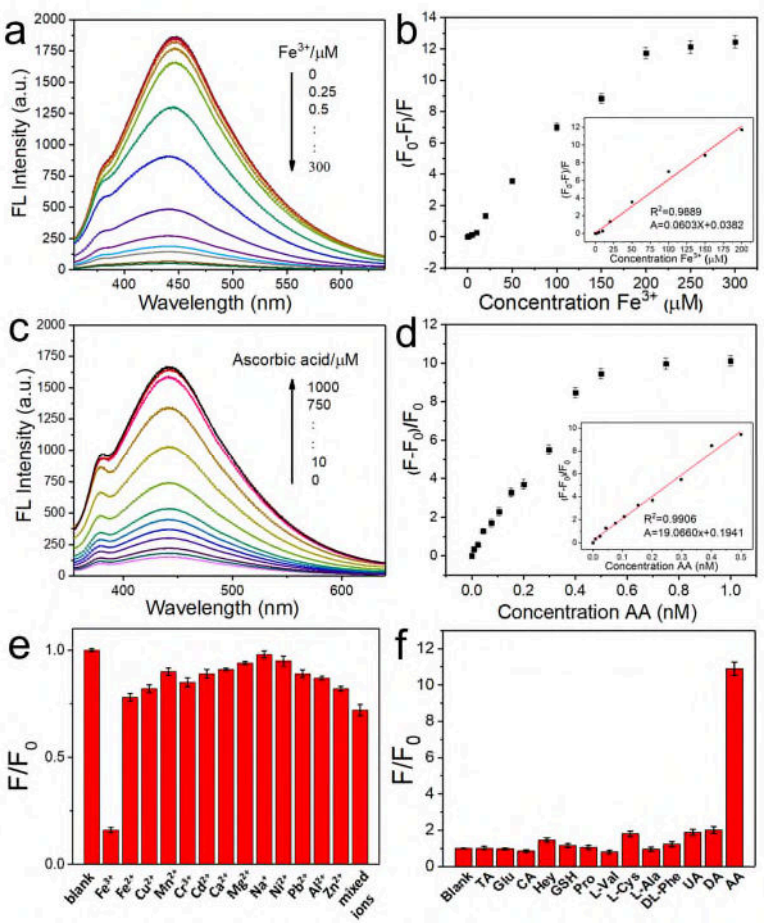

Fig. 5. (a) UV–vis absorption spectra of GDYO-QDs (black) and Fe^{3+} (blue), fluorescence spectrum of GDYO-QDs (red). (b) The fluorescence lifetime of GDYO-QDs without Fe^{3+}, with 50 and 100 μmol L^{-1} Fe^{3+}. (c) Quench efficient of observed (Q_{obsd}) and corrected (Q_{cor}) fluorescence of GDYO-QDs with Fe^{3+}, which was calculated according to equation: $Q_F = (F_0 - F)/F_0$. Inset: Parameters used for the correction of the inner filter effect: I_0 represents the excitation beam; s is the thickness of the excitation beam (0.10 cm); g is the distance between the edge of the excitation beam and the edge of the cuvette (0.40 cm); d is the width of the cuvette (1.00 cm) and F is the observed fluorescence beam. (d) A plot of $(\alpha hv)^{1/2}$ versus photon energy (Eg) of GDYO-QDs, and the dotted line is a linear fitting. (e) XPS valence band spectrum of GDYO-QDs, the dotted line is a linear fitting. (f) Schematic diagram of PET process mechanism between Fe^{3+} and GDYO-QDs.

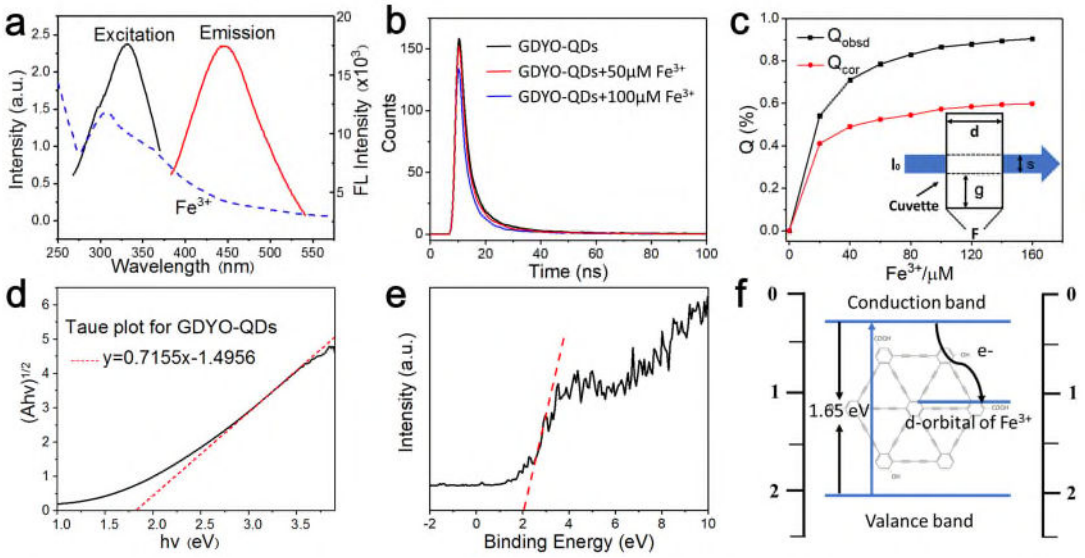

Table 1. Recoveries of Fe^{3+} in human serum samples and validation results of the analyte by atomic absorption spectrometry (AAS) method compared with the presented method.(n=3).

Serum sample	Added Fe^{3+} ($\mu M\ L^{-1}$)	Found Fe^{3+} ($\mu M\ L^{-1}$)	Recovery (%)	Found $Fe^{3+}$by AAS ($\mu M\ L^{-1}$)	Recovery by AAS(%)	T-test [a]
1 [b]	-	65.53± 1.65	-	65.12±1.44	-	0.38
	50	117.43±1.73	101.64	115.24±1.86	100.11	0.57
	100	169.94±2.42	102.66	163.53±2.24	99.04	0.62
	150	220.58±3.25	102.34	212.47±3.64	98.77	0.51
2 [b]	-	23.43± 0.84	-	23.97±0.78	-	0.64
3 [b]	-	15.83± 0.48	-	16.31±0.51	-	0.83
4 [b]	-	49.58± 1.25	-	48.66±1.13	-	0.46
5 [b]	-	70.43± 1.57	-	72.66±1.21	-	0.77
6 [b]	-	32.85± 1.07	-	31.62±0.99	-	0.72
7 [b]	-	45.74± 1.27	-	46.64±1.08	-	0.59

[a] T-Critical= 3.72 for n =3 and P = 0.05

[b] Obtained from Qingdao Central Hospital

Supporting Information：

Subsequent monitoring of ferric ion and ascorbic acid using graphdiyne quantum dots-based optical sensors

Qiang Bai[a,c], Chaoyang Zhang[b], Long Li[b], Zhiling Zhu[a], Lina Wang[b,*], Fuyi Jiang[c], Manhong Liu[a], Zhaobo Wang[a], William W. Yu [a,d], Fanglin Du[a,*], Zhugen Yang[e,*], Ning Sui[a,*]

[a] *College of Materials Science and Engineering, Qingdao University of Science and Technology, Qingdao 266042, China*
[b] *College of Environment and Safety Engineering, Qingdao University of Science and Technology, Qingdao, 266042, China.*
[c] *School of Environment and Material Engineering, Yantai University, Yantai, 264005, Shandong, China*
[d] *Department of Chemistry and Physics, Louisiana State University Shreveport, LA 71115, USA*
[e] *Cranfield Water Science Institute, Cranfield University, Milton Keynes, MK43 0AL, United Kingdom*

* Corresponding authors: suining@qust.edu.cn (N. Sui), lnwang2006@163.com (L.N. Wang), dufanglin@qust.edu.cn (F.L. Du), zhugen.yang@cranfield.ac.uk (Dr Z. Yang)

Contents

Quantum yields (QYs) measurements.

QYs of the GDYO-QDs was determined by using quinine sulfate (QY_R=0.560 in water) as the standard sample and were calculated according to the following equation:

$$QY_X = QY_R \frac{I_X}{I_R}\frac{A_R}{A_X}\frac{\eta_X^2}{\eta_R^2}$$

where QY is the quantum yield, the subscript "R" refers to the known QY standard of quinine sulfate and “X” means number of samples, I is the measured integrated emission intensity, A is the ultraviolet absorbance and η is the refractive index.

Optimization of the testing conditions.

A fluorescence sensor based GDYO-QDs were established for Fe^{3+} and AA detection. The experimental conditions including the pH value of the assay and the reaction time were investigated and optimized. We used B-R buffer as a medium to detect fluorescence spectra of GDYO-QDs under different pH value from 2.0 to 10.0 (Figure S6a, b). The fluorescence intensity of GDYO-QDs reached the optimum at pH = 6.0. After the addition Fe^{3+}, sharp decreases of the fluorescence intensity were observed at each pH value (Figure S7). The largest change of the fluorescence intensity occurred at pH = 6.0 in the absence and presence of Fe^{3+}, which indicates that the best quenching effect occurs when pH = 6.0. Figure S8a shows the time-dependent fluorescence spectra of GDYO-QDs (0.1mg mL^{-1}) mixed with 200 μmol L^{-1} of Fe^{3+}. The fluorescence intensity of GDYO-QDs decreased with the increase of reaction time and became insignificantly after 20 minutes (Figure S8b). Therefore, the optimum experimental conditions are pH = 6.0 and reaction time of 20 min. As shown in Figure S9a, the quenching efficiency of GDYO-QDs by different concentrations of Fe^{3+} were about the same. On this premise, AA investigated the recovery under different concentrations of Fe^{3+}, and the recovery was the best when Fe^{3+} was 200 μmol L^{-1} (Figure S9b).

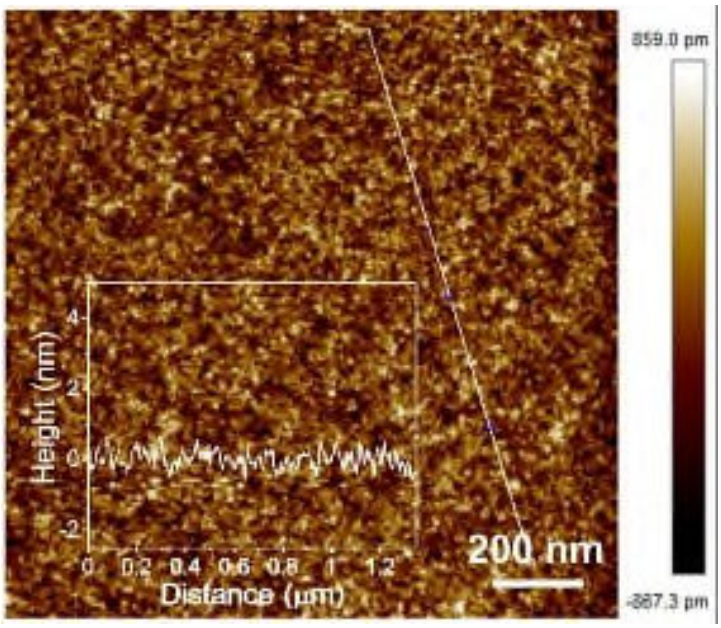

Fig. S1. AFM image of naked substrate.

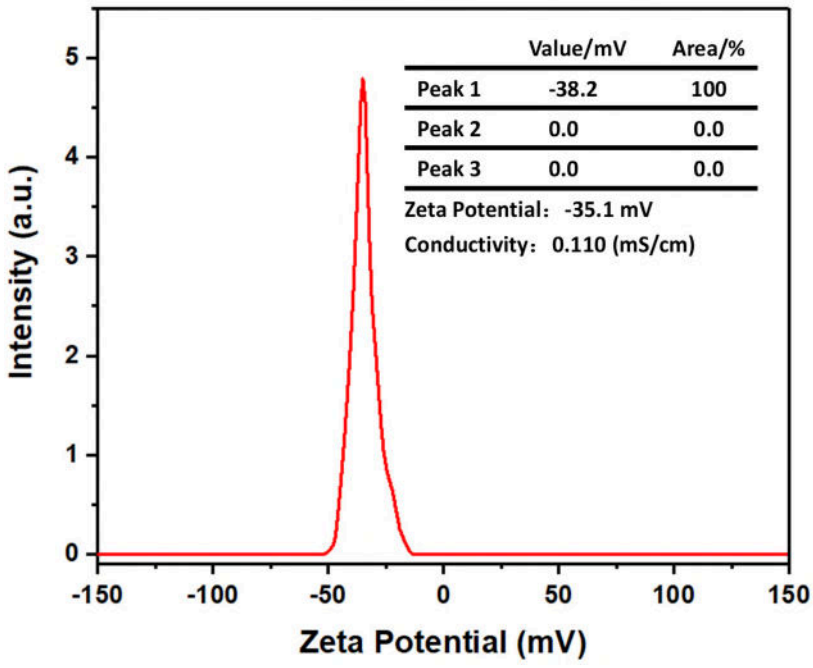

Fig. S2. Zeta potential of GDYO-QDs solution.

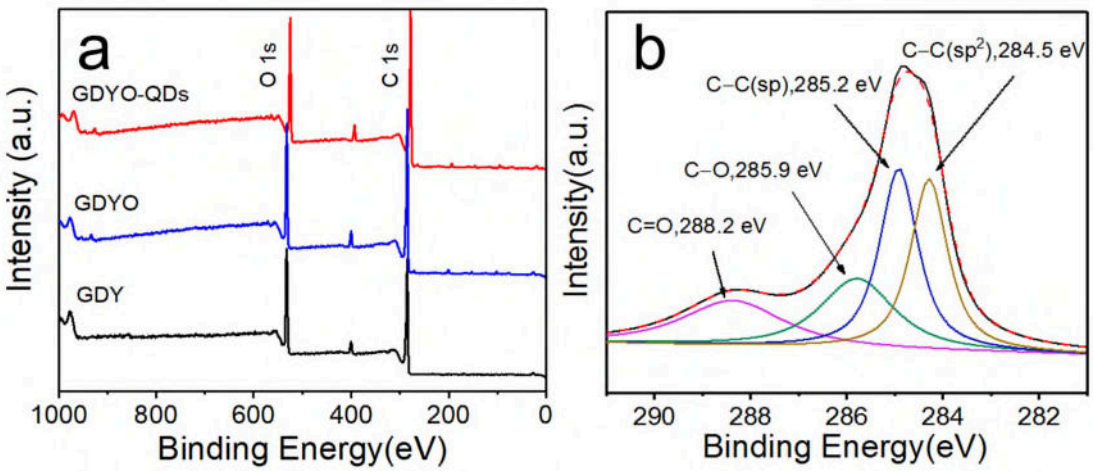

Figure S3. (a) XPS spectra of GDY, GDYO and GDYO-QDs. (b) High-resolution C1s spectra of GDYO

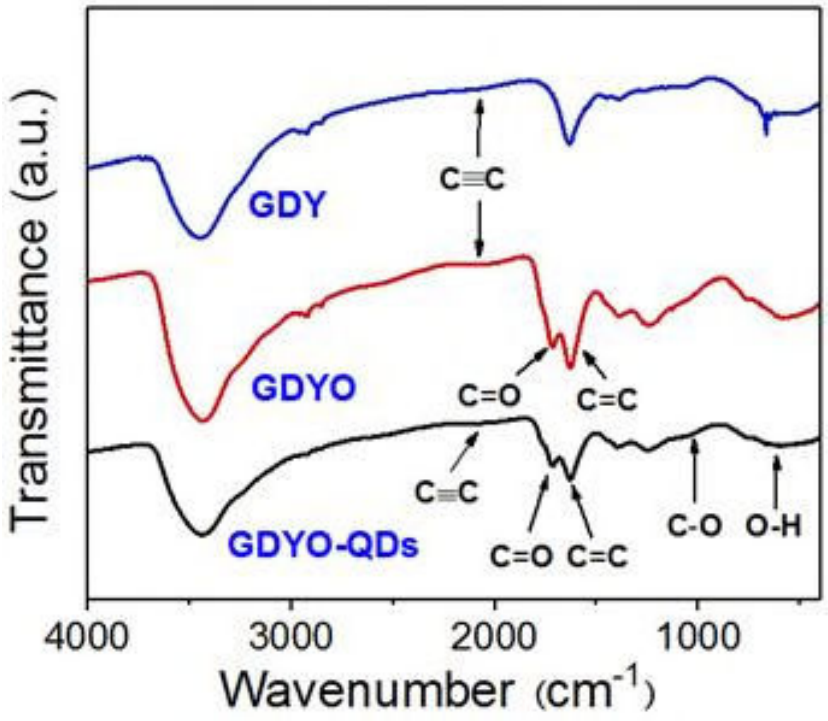

Fig. S4. FT-IR spectra of GDY, GDYO and GDY-QDs.

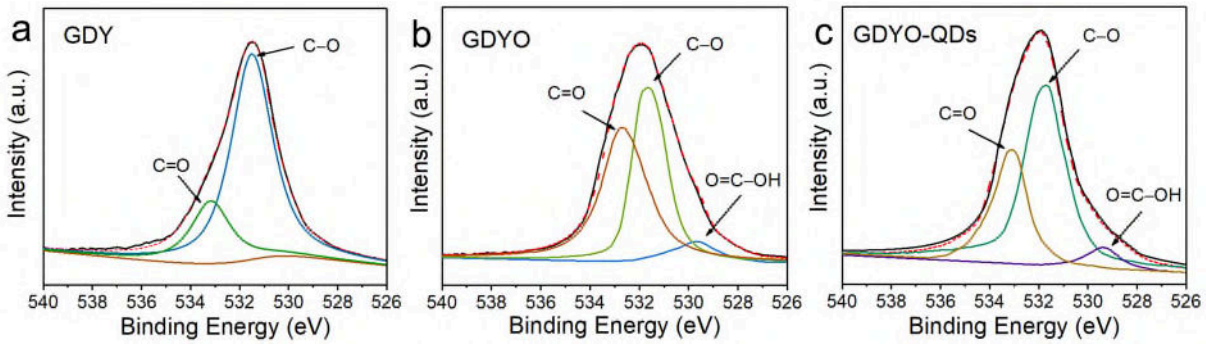

Fig. S5. The O1s spectra of (a) GDY, (b) GDYO and (c) GDYO-QDs.

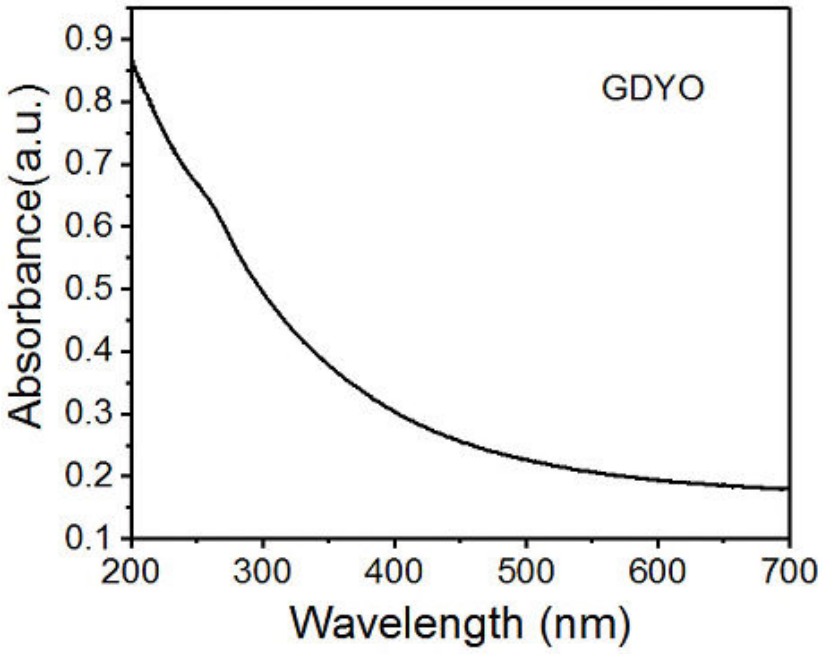

Fig. S6. UV−vis absorption spectra of GDYO.

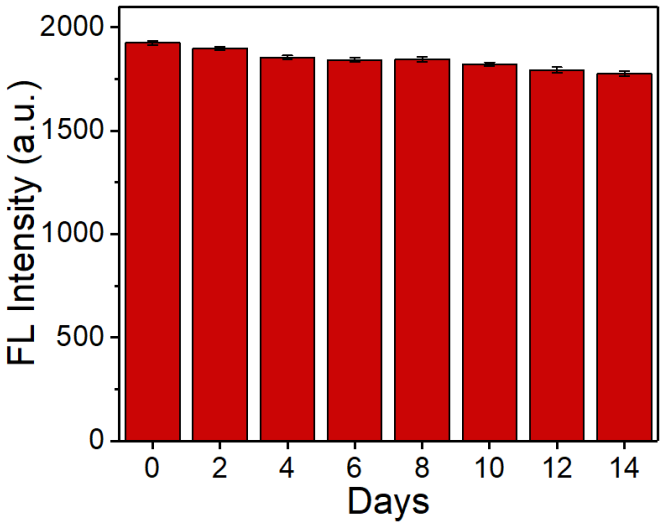

Fig. S7. The fluorescence stability of GDYO-QDs within 14 days.

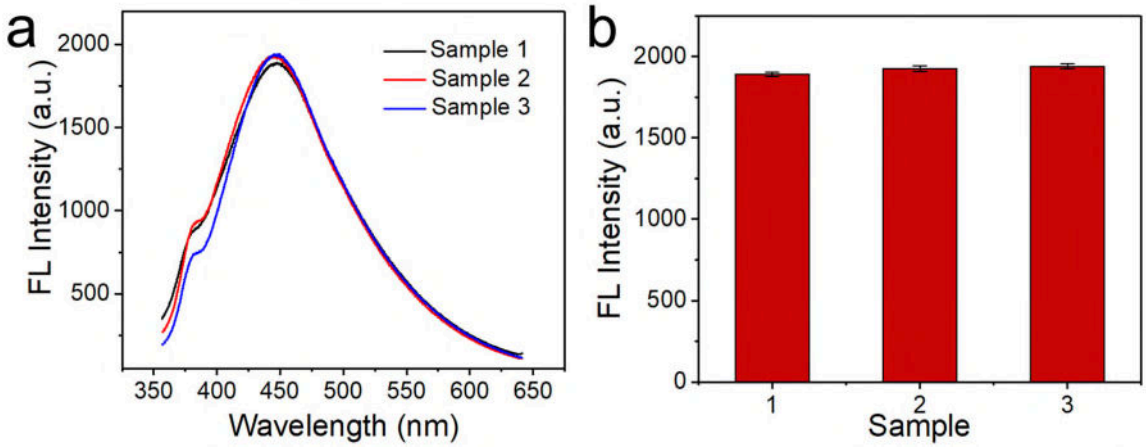

Fig. S8. (a) Fluorescence spectra of different batches of GDYO-QDs. (b) Histogram of fluorescence intensity comparison.

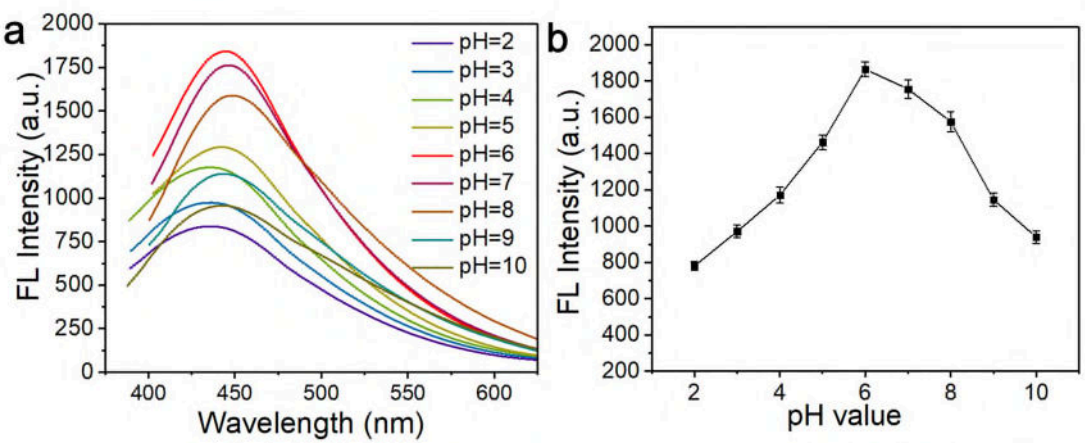

Fig. S9 (a) Fluorescence spectra of GDYO-QDs under different pH.

(b) Effect of pH on the GDYO-QDs

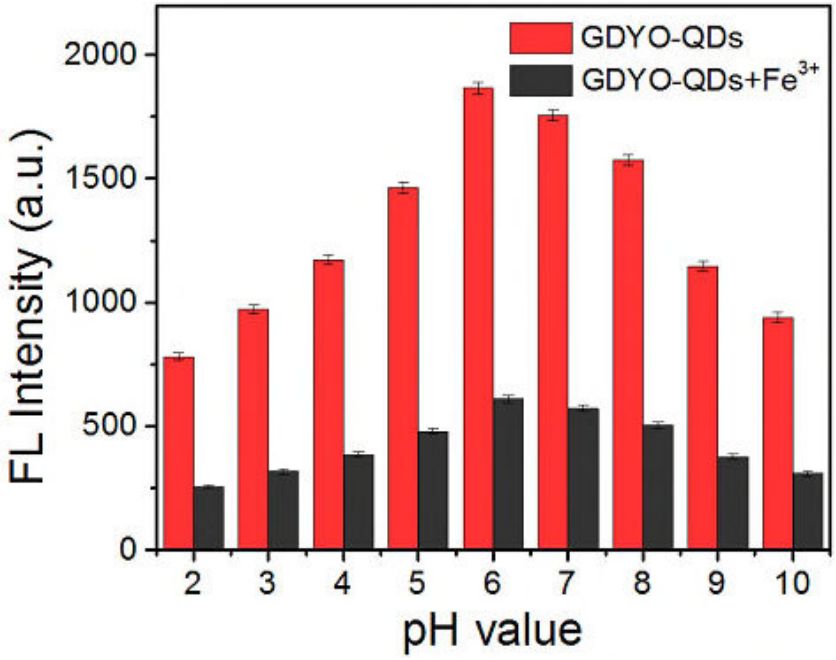

Fig. S10. The fluorescence response of GDYO-QDs without and with 50 μmol L^{-1} Fe^{3+} at different pH values.

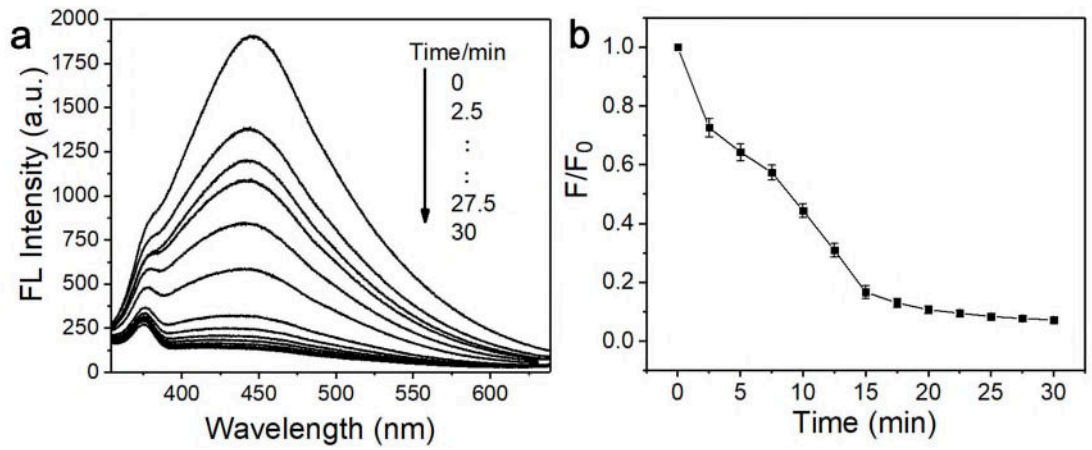

Fig. S11. (a) Fluorescence quenching of GDYO-QDs by 200 μmol L^{-1} Fe^{3+} in B-R buffer (pH = 6) as a function of time (λ_{ex} = 331 nm). (b) The change of F_0/F with the reaction time.

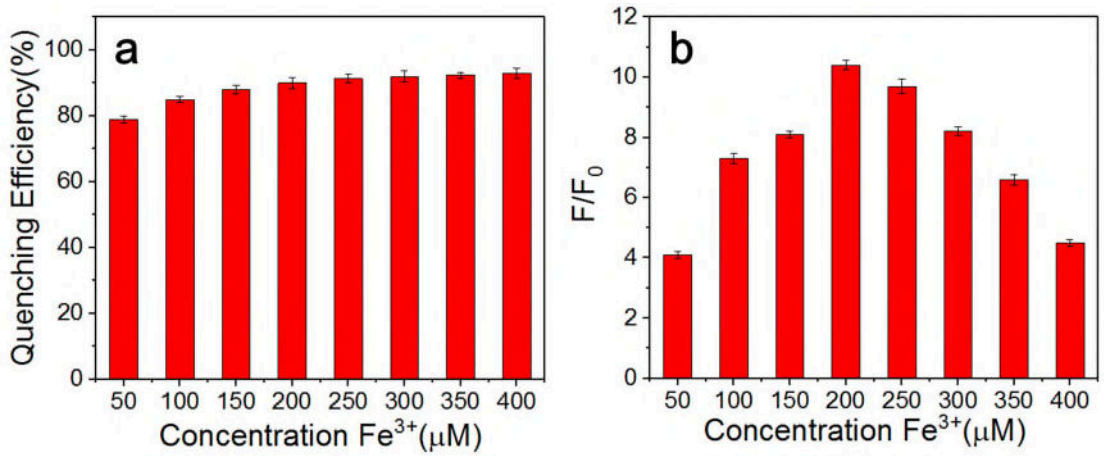

Fig. S12. (a) The quenching efficiency of GDYO-QDs to various concentrations of Fe^{3+}. (b) The sensitivity of AA (500 μmol L^{-1}) response to different concentrations of Fe^{3+}. (F_0 and F are the fluorescence intensities of GDYO-QDs /Fe^{3+} in the absence and presence of AA, respectively)

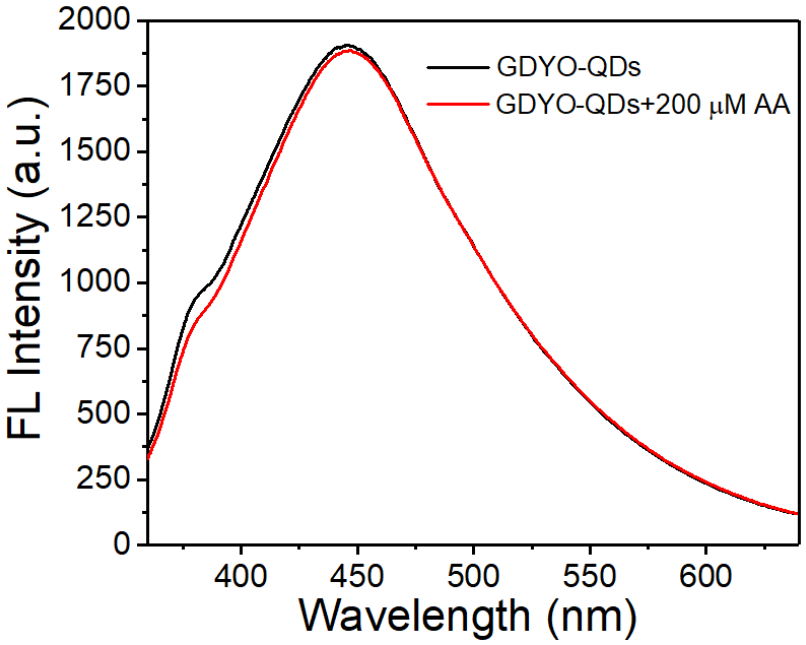

Fig. S13. Fluorescence spectra of GDYO-QDs and GDYO-QDs with AA.

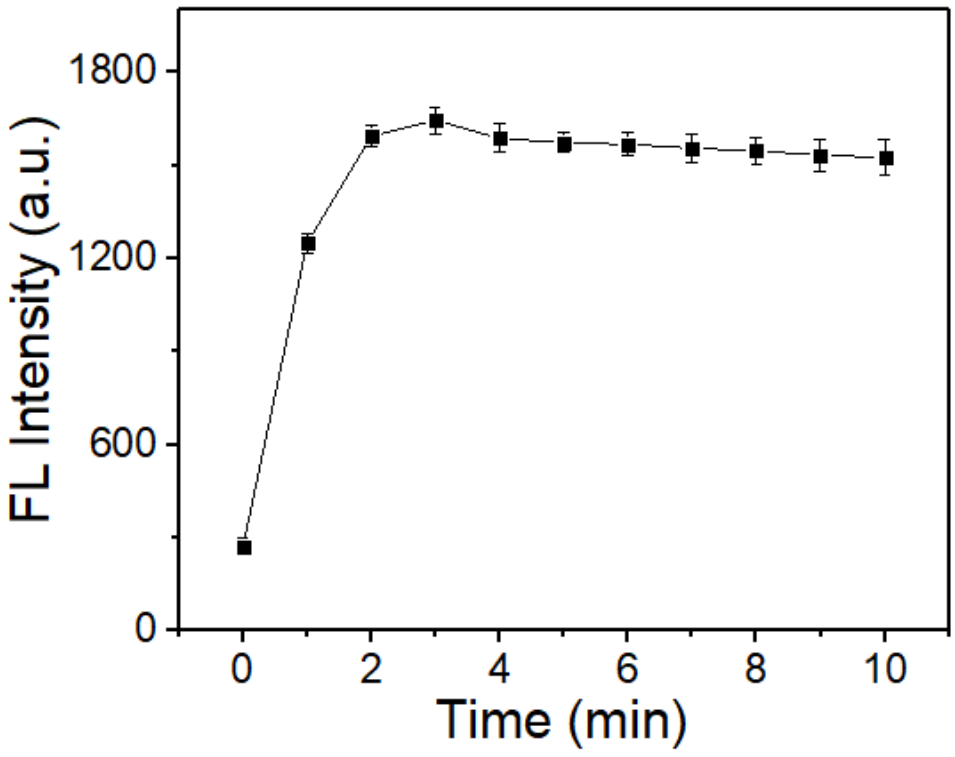

Fig. S14. Fluorescence intensity of GDYO-QDs / Fe^{3+} after reaction with AA (400 μmol L^{-1}) for different times.

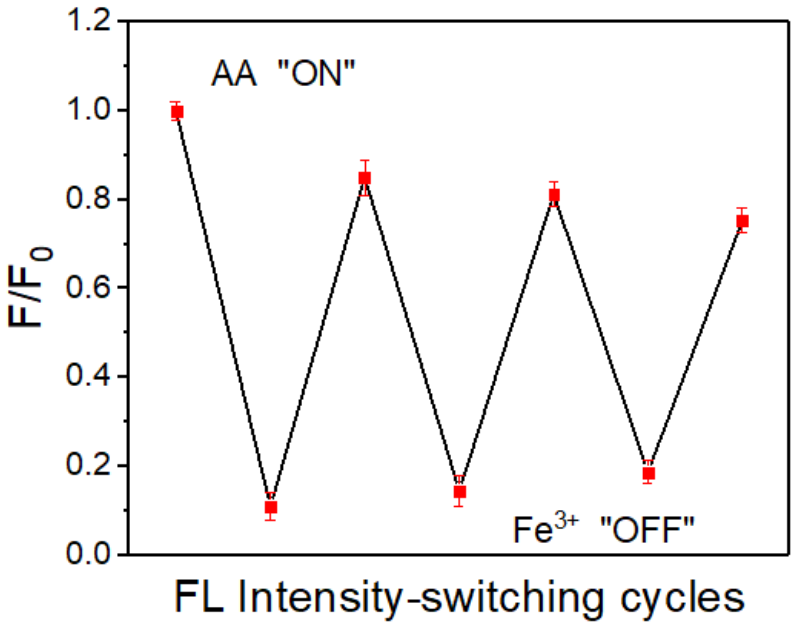

Fig. S15. Reversible of GDYO-QDs upon alternate addition of Fe^{3+} and AA.

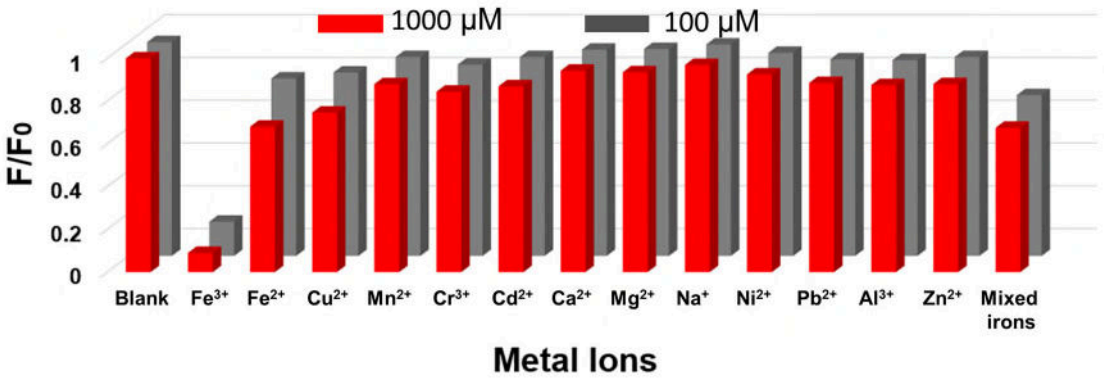

Fig. S16. Selective response of aqueous GDYO-QDs towards different metal ions (λ_{ex} = 331 nm). F_0 and F are the fluorescence intensities of GDYO-QDs at 446 nm in the absence and presence of metal ions, respectively.

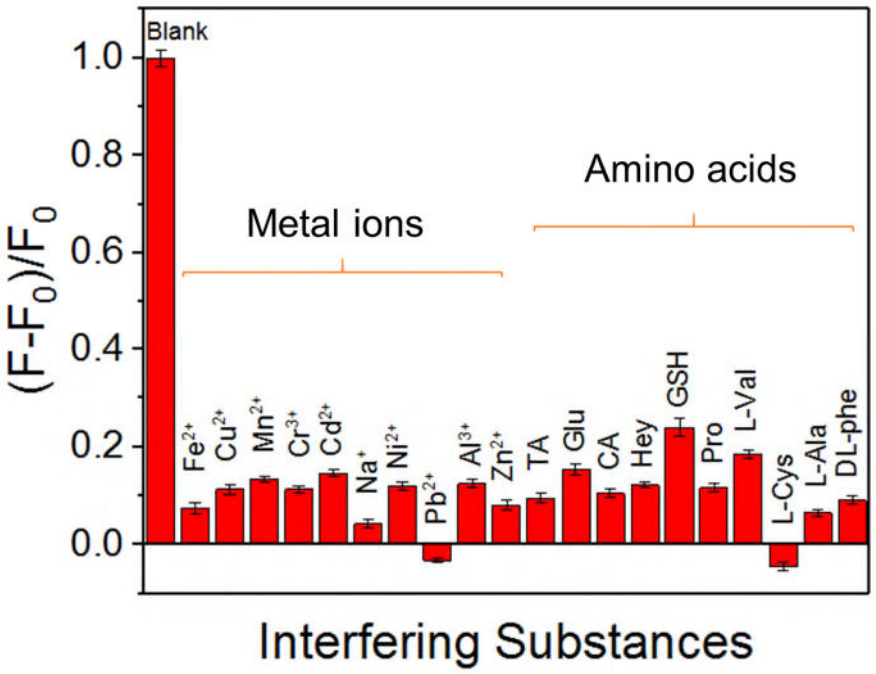

Fig. S17. An interference study of GDYO-QDs sensor for Fe^{3+} (200 μmol L^{-1}) and AA (400 μmol L^{-1}) premixed with other interfering substances (400 μmol L^{-1}).

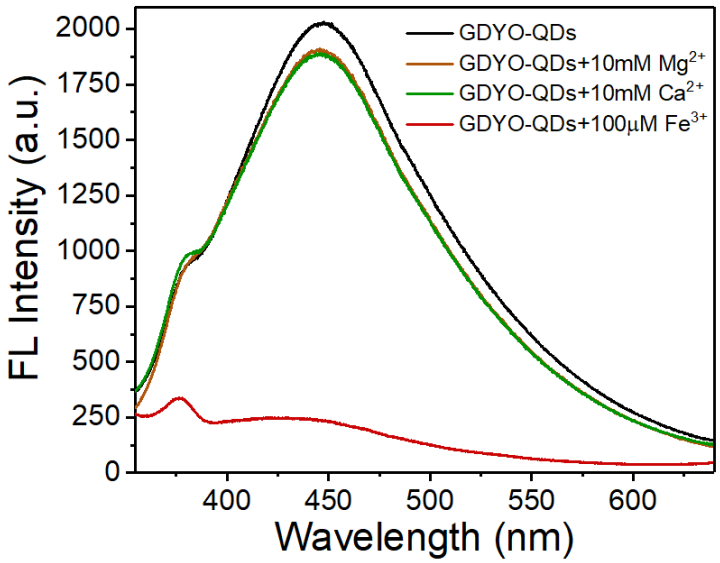

Fig. S18. Fluorescence response of GDYO-QDs in the presence of 10 mmol L^{-1} of Mg^{2+}, 10 mM of Ca^{2+} and 100 μM of Fe^{3+}.

Table S1. Elemental analysis of the GDY, GDYO and GDYO-QDs by XPS

Element	**C**	**O**
GDY(%)	78.78	21.22
GDYO (%)	73.26	26.74
GDYO-QDs(%)	68.43	31.57

Table S2. Performance of the new sensor (GDYO-QDs) compared with other reported fluorescence sensors for analysis of Fe^{3+} and AA.

Probe	Fe^{3+}			AA		Ref.
	Liner Range/μM	LOD (μM)	Quenching Mechanism	Liner Range/μM	LOD (μM)	
MIL-53(Fe)-$(OH)_2$	5~200	1.7	PET	-	-	[1]
b-CDs	1~60	0.28	PET	-	-	[2]
ZnMOF-74	0.1~100	0.04	PET	-	-	[3]
CNQDs	2~200	1.0	PET	-	-	[4]
MPS	0~100	1.54	SQ a	-	-	[5]
g-CN QDs	0.2~60	0.023	IFE	-	-	[6]
MIL- 53(Al)	3~200	0.9	PET	-	-	[7]
Bi_2S_3-TiO_2	30 ~ 5000	0.1173	PET	-	-	[8]
N,S-doped CDs	-	-	PET	10~200	4.69	[9]
GDQs	-	-	FRET	1.0~95	0.2	[10]
GSH-Ag	-	-	-	4~300	0.1	[11]
g-C_3N_4 NNs	0.5~30	0.18	IFE, PET	0.2~112.5	0.086	[12]
GDYO-QDs	0.25~200	0.095	SQ, IFE, PET	10~500	2.5	This work

Table S3. IFE of Fe^{3+} on the fluorescence of GDYO-QDs

Fe^{3+}/μM	A_{ex}	A_{em}	CF	F_{obsd}	F_{cor}	Q_{obsd}	Q_{cor}
0	0.175	0.139	1.1064	1867	2613.4	0	0
20	0.314	0.236	1.7005	906	1540.6	0.5417	0.4105
40	0.538	0.341	2.4607	541	1331.2	0.7102	0.4906
60	0.668	0.446	3.0989	401	1242.7	0.7852	0.5245
80	0.768	0.553	3.7373	318	1188.5	0.8297	0.5452
100	0.870	0.642	4.4296	252	1116.3	0.8650	0.5729
120	0.918	0.731	5.0028	226	1085.6	0.8789	0.5847
140	0.976	0.820	5.7399	197	1060.3	0.8945	0.5943
160	1.0288	0.903	5.9969	175	1049.5	0.9043	0.5984

Table S4. Recoveries of AA in human serum samples (n=3).

Sample	**Added ($\mu M\ L^{-1}$)**	**Found ($\mu M\ L^{-1}$)**	**Recovery (%)**	**RSD (%)**
1	0	0	-	-
2	50	48.87±0.70	97.74	1.28
3	200	204.54±4.65	102.27	1.97
4	400	394.28±8.80	98.57	2.12

Reference

[1] Zhao Y, Ouyang H, Feng S, Luo Y, Shi Q, Zhu C, et al. Rapid and selective detection of Fe (III) by using a smartphone-based device as a portable detector and hydroxyl functionalized metal-organic frameworks as the fluorescence probe. Anal Chim Acta 2019;1077:160-6.

[2] Xu X, Ren D, Chai Y, Cheng X, Mei J, Bao J, et al. Dual-emission carbon dots-based fluorescent probe for ratiometric sensing of Fe(III) and pyrophosphate in biological samples. Sensors and Actuators B: Chemical 2019;298.

[3] Hou L, Song Y, Xiao Y, Wu R, Wang L. ZnMOF-74 responsive fluorescence sensing platform for detection of Fe^{3+}. Microchemical Journal 2019;150.

[4] Li S, Li Y, Cao J, Zhu J, Fan L, Li X. Sulfur-Doped Graphene Quantum Dots as a Novel Fluorescent Probe for Highly Selective and Sensitive Detection of Fe^{3+}. Analytical Chemistry 2014;86:10201-7.

[5] Wang X, Wang H, Feng S. A novel thiophene functionalized silicon-cored compounds: Aggregation-induced emission enhancement and aqueous fluorogenic Fe^{3+} probes in bovine serum albumin. Sensors and Actuators B: Chemical 2017;241:65-72.

[6] Li Y, Cai J, Liu F, Yu H, Lin F, Yang H, et al. Highly crystalline graphitic carbon nitride quantum dots as a fluorescent probe for detection of Fe(III) via an innner filter effect. Microchim Acta 2018;185:134

[7] Zhang Y-L, Wang L, Zhang H-C, Liu Y, Wang H-Y, Kang Z-H, et al. Graphitic carbon quantum dots as a fluorescent sensing platform for highly efficient detection of Fe^{3+} ions. RSC advances 2013;3:3733-8.

[8] Syal A, Sud D. Development of highly selective novel fluorescence quenching probe based on Bi_2S_3-TiO_2 nanoparticles for sensing the Fe(III). Sensors and Actuators B: Chemical 2018;266:1-8.

[9] Luo, X. L.; Zhang, W. G.; Han, Y.; Chen, X. M.; Zhu, L.; Tang, W. Z.; Wang, J. L.; Yue, T. L.; Li, Z. H. N,S co-doped carbon dots based fluorescent “on-off-on” sensor for determination of ascorbic acid in common fruits. Food Chem. 2018, 258, 214–221.

[10] Gao, Y.; Yan, X. L.; Li, M.; Gao, H.; Sun, J.; Zhu, S. Y.; Han, S.; Jia, L. N.; Zhao, X. E.; Wang, H. A “turn-on” fluorescence sensor for ascorbic acid based on graphene quantum dots via fluorescence resonance energy transfer. Anal. Methods 2018, 10, 611–616.

[11] Li, N.; He, Y.; Ge, Y. L.; Song, G. W. “Turn-Off-On” Fluorescence Switching of Ascorbic Acid-Reductive Silver Nanoclusters: a Sensor for Ascorbic Acid and Arginine in Biological Fluids. J. Fluoresc. 2017, 27, 293–302.

[12] X. Guo, G. Yue, J. Huang, C. Liu, Q. Zeng, L. Wang, Label-Free Simultaneous Analysis of Fe(III) and Ascorbic Acid Using Fluorescence Switching of Ultrathin Graphitic Carbon Nitride Nanosheets, Acs Applied Materials & Interfaces. 10 (2018) 26118-26127.